Methods in Oceanography 10 (2014) 104–121

Contents lists available at ScienceDirect

Methods in Oceanography

journal homepage: www.elsevier.com/locate/mio

Full length article

The SailBuoy remotely-controlled unmanned vessel: Measurements of near surface temperature, salinity and oxygen concentration in the Northern Gulf of Mexico

Mahmud Hasan Ghani [a,b], Lars R. Hole [a,*], Ilker Fer [b,c], Vassiliki H. Kourafalou [d], Nicolas Wienders [e], HeeSook Kang [d], Kyla Drushka [f], David Peddie [c]

[a] Norwegian Meteorological Institute, Bergen, Norway
[b] Geophysical Institute, University of Bergen, Bergen, Norway
[c] Christian Michelsen Research AS, Bergen, Norway
[d] University of Miami/RSMAS Miami, FL, USA
[e] Florida State University, Earth, Ocean and Atmospheric Science, Tallahassee, FL, USA
[f] Applied Physics Laboratory, University of Washington, Seattle, WA, USA

ARTICLE INFO

Article history:
Received 20 February 2014
Received in revised form
8 August 2014
Accepted 19 August 2014
Available online 16 September 2014

Keywords:
SailBuoy
SST
Salinity
Dissolved oxygen
River plumes
Gulf of Mexico

ABSTRACT

An experimental deployment of a new type of unmanned vessel is presented. The Christian Michelsen Research SailBuoy, a remotely-controlled surface vehicle, sampled near-surface properties during a two-month mission in the northern Gulf of Mexico in March–May, 2013. Averaged over the entire deployment, the vessel speed over ground was 42 ± 30 cm s^{-1} (± one standard deviation) with a maximum of 180 cm s^{-1}. During the 62 days of the mission, the SailBuoy covered a total range of approximately 400 km in both meridional and zonal directions, with a cumulative total distance of approximately 2400 km. Three parameters were recorded: sea surface temperature, conductivity, and dissolved oxygen. Observed surface temperature and salinity records are compared with remote sensing data and the salinity fields from a regional ocean modeling system, respectively. The absolute difference between remote sensing data to surface

* Corresponding author. Tel.: +47 91769141.
E-mail address: lrh@met.no (L.R. Hole).

http://dx.doi.org/10.1016/j.mio.2014.08.001

temperature is on an average approximately 0.5 °C. The comparison with the full Gulf of Mexico and the nested Northern Gulf of Mexico HYCOM models demonstrates the validity and usefulness of SailBuoy measurements and the instrument's utility in evaluating fields produced by ocean models having different attributes. The potential of the SailBuoy for mapping a large-scale river plume, which would be challenging or costly with conventional ship surveys and/or remote sensing, is demonstrated.

1. Introduction

The surface of the ocean is a complex boundary across which momentum, heat and gas exchanges take place. Near surface properties, such as the sea surface temperature (SST), and sea surface salinity (SSS) play a crucial role in controlling the exchange between the ocean and the atmosphere, as well as in influencing the weather and large scale ocean and atmospheric circulation. Near-surface dissolved oxygen concentration (oxygen or O_2 hereafter) is a component that responds to both physical changes (as a result of the temperature and salinity dependence of O_2 solubility and ventilation) as well as biological changes (such as production and consumption, effects of stratification changes on vertical nutrient supply) and therefore can potentially be used as a sensitive indicator of environmental change in the ocean (Joos et al., 2003). Measurements of near-surface properties of seawater are therefore crucial, not only for understanding the physical mechanisms and processes, but also to constrain and calibrate satellite data and numerical models.

During the 1990s, independent ocean observing systems such as buoys were outfitted with CT (conductivity and temperature) sensors and started transmitting T and salinity S using different means of radio or satellite communication. Such platforms now typically use the Iridium System, allowing for two-way communications and a wider bandwidth, and can carry many more sensors such as O_2, rain, sound, Chlorophyll, Chromophoric Dissolved Organic Matter (CDOM), and Acoustic Doppler Current Profilers. Körtzinger et al. (2005) reported the first study results from two profiling floats equipped with optode sensors for oxygen measurements. For the last few decades, rapid technological advancement has resulted in a wide range of autonomous (or semi-autonomous) ocean observing systems and Lagrangian systems equipped with purpose-built sensors. By "autonomous", we mean an unmanned vessel that can navigate to a certain location, or way point, using an auto-pilot system. Although a standard observation system is difficult to define, the remote operational procedure classifies the system as an autonomous system. The first vessel representative of the group of autonomous surface vessels was "ARTEMIS". Developed through the MIT Sea Grant College program in 1993, it resembled a fishing trawler and was capable of testing the navigation and control systems (Manley, 1997). Other examples were the "Dolphin" developed by the University of Rostock (Germany) (Caccia et al., 2008), the catamaran "Delfim" (Pascoal et al., 2000), the "Caravela" boat developed by the DSOR lab of Lisbon ISTISR (dsor.isr.ist.utl.pt/Projects/Caravela/), and the autonomous catamaran "Charlie" of CNR-ISSIA Genova, Italy (Caccia et al., 2005). The Wave Glider designed by Liquid Robotics, Sunnyvale California, is a wave-powered vehicle that can be outfitted with sensors and deployed on long distance missions that can last many months (Lenain and Melville, 2014). The Wave Glider is known as the first unmanned autonomous marine robot to use the ocean's endless supply of wave energy for propulsion (http://liquidr.com/technology/wave-glider.html). Very recently, new autonomous systems—either wind-propelled like the SailDrone (http://mstfoundation.org/story/Saildrone), using solar energy like the C-Enduro (http://www.asvglobal.com/science-survey/c-enduro), or using batteries like the "Pioneer" (http://www.njordworks.com/)—have appeared on the market. There have been very few evaluations or publications on these systems, and our article aims to document one of these new vehicles, the Christian Michelsen Research (CMR) SailBuoy (http://www.sailbuoy.no) (Fer and Peddie, 2012).

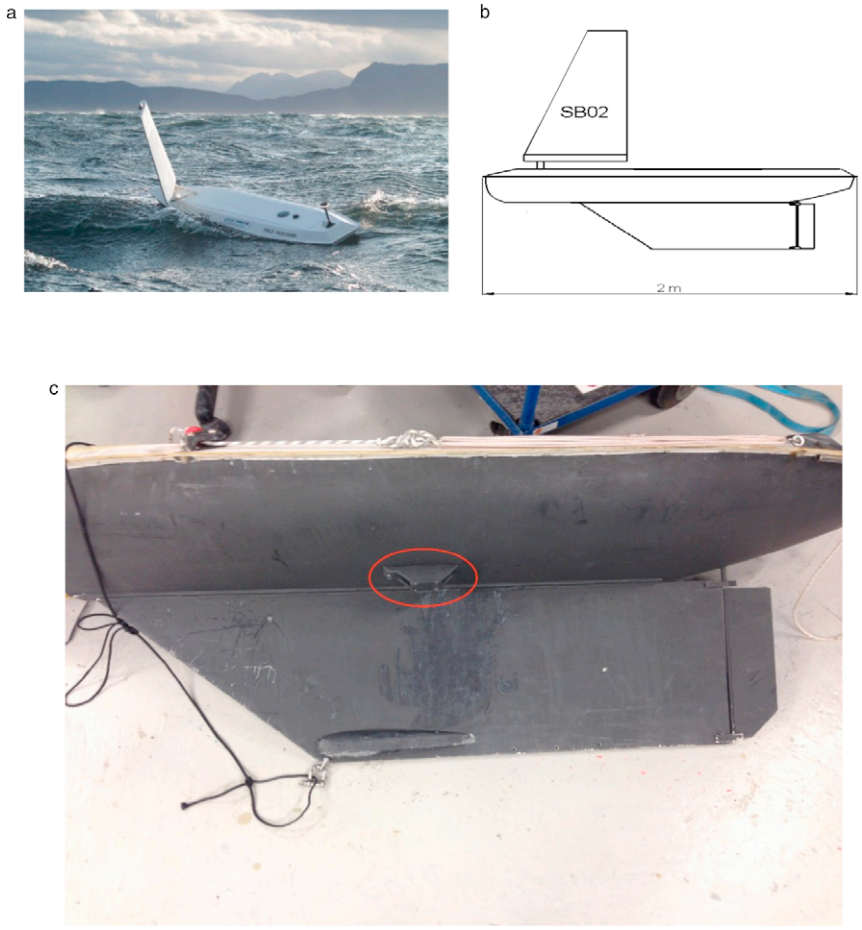

Fig. 1. (a) The SailBuoy during a mission, (b) outline of the SailBuoy, (c) detail of the SailBuoy showing the CT sensor in the red oval. (For interpretation of the references to color in this figure legend, the reader is referred to the web version of this article.)

Autonomous observational systems provide an advanced method to accurately and routinely sample large ocean areas for the aforementioned hydrographic properties. Most automatic remote systems used for *in situ* exploration of the oceans are either geo-stationary, moored, or drifting, such as anchored platforms, drifting buoys or land-based platforms. The CMR SailBuoy (from here on referred to as the SailBuoy) is a new oceanic surface system that navigates without a propeller (Fig. 1). It uses wind power to sail toward pre-defined waypoints making it an attractive alternative to freely drifting surface buoys.

A recent focus of oceanographic research in the Gulf of Mexico (GoM) is the interactions between large-scale circulation in the GoM and the DeSoto Canyon, how external events such as eddies and winds influence circulation and upwelling in the canyon, and what controls sediment transport and resuspension (Deep-C project). Previous efforts have contributed greatly to our knowledge of the region. Hamilton et al. (2000) and Hamilton and Lee (2005), using a set of moorings, drifters and hydrographic cruises, report that the presence of cyclones and anticyclones over the lower Mississippi–Alabama slope is strongly influenced by the position of the Loop Current and its associated eddies (warm anti-cyclonic core or cyclonic frontal eddies). The consequence is usually an eastward surface jet on the upper slope, which can follow the rim of the canyon or meander across the slope.

Table 1
Technical specifications of the SailBuoy system.

Length	2 m
Draft	30 cm
Displacement	60 kg
Payload	10 kg / 60 l
Speed	1–2 knots
Navigable wind speed	3–20 m/s
Operational time	1 year
Communication	Iridium SBD

Vukovich (2007) provides a climatology describing the frequency of intrusion of Loop Current Water onto the shelf and ring path, speed and dissipation, using satellite remote sensing and *in situ* data. One conclusion is that Cold Core Rings were the primary driver of mass and heat redistribution in the eastern GOM. Huh et al. (1981) describe an intrusion of loop current water up the De Soto Canyon and onto the West Florida continental shelf to within 8 km of the shore in February 1977. The duration of the event was 18 days, with across shelf velocities of about 20 cm s^{-1}.

Wang et al. (2003) using moorings, satellite data and model results showed that there are two dominant modes of circulation in the DeSoto Canyon region: a "single-eddy" mode, in which currents are concentrated at the foot of the canyon, and an "eddy-pair" mode, in which one eddy is at the foot of the canyon and the other, a counter-rotating eddy, is over the head of canyon. The satellite-derived velocity field is shown to contain both the first and second modes although the satellite field does not adequately resolve the velocity structures over the slope where bathymetry and friction likely play a role. Thus, *in situ* observations are crucial to obtain in order to describe the process of connectivity and exchange from the Gulf to the canyon to the shelf.

Here, we present results from an experiment that took place in the northern GoM, from March 15 to May 15, 2013 (62 days). The experiment had the following specific objectives: (1) monitoring of the physical properties of the GoM (SST, SSS and O_2); (2) demonstrating the utility of using a remotely controlled vehicle for reliable data collection; and (3) providing a system for validation of relevant remote sensing data and model simulations.

2. Materials and methods

2.1. The CMR SailBuoy

Being 100% wind driven and using battery power only for automatic tacking, the CMR SailBuoy system is capable of carrying out long missions for up to 6 months. Sensors and the communication system have a separate battery. Typical capacity is 240 Wh, 20 Ah at 12 V.

It can both receive navigational instructions and transmit data in real time via 2-way Iridium communication. A full array of sensors can be used for applications in oceanography, meteorology, marine mammal monitoring, algae surveys, oil tracking, and wave measurements. The vessel can be easily deployed and retrieved by untrained personnel, and is not logistically demanding since the operator does not have to travel to the research site. The basic technical specifications are listed in Table 1.

The SailBuoy was deployed South of Cape San Blas (Northeastern GoM) on March 15, 2013 and was recovered on May 15 after a mission that lasted 62 days, covering a cumulative distance of about 2400 km in the GoM (Fig. 2). The SailBuoy was first set to follow the topographic features of the Northern De Soto Canyon. The goal here was to address the possibility of sampling cross-shelf flows. Later, the SailBuoy was kept stationary for a few days at the head of the Canyon, to monitor potential upwelling events which can occur under specific upwelling conditions. Halfway into the deployment, it was directed southwest to map the location of the Mississippi River (MR) plume. For this experiment, the SailBuoy was equipped with a low-drag, fast-response conductivity–temperature (G-CTD) sensor (Schmitt and Petitt, 2006) manufactured by Neil Brown Ocean Sensors, Inc. (NBOSI), and an oxygen optode (AS4835) manufactured by Aanderaa Data Instruments, Xylem Inc. The details of the sensors are summarized below, following Fer and Peddie (2012).

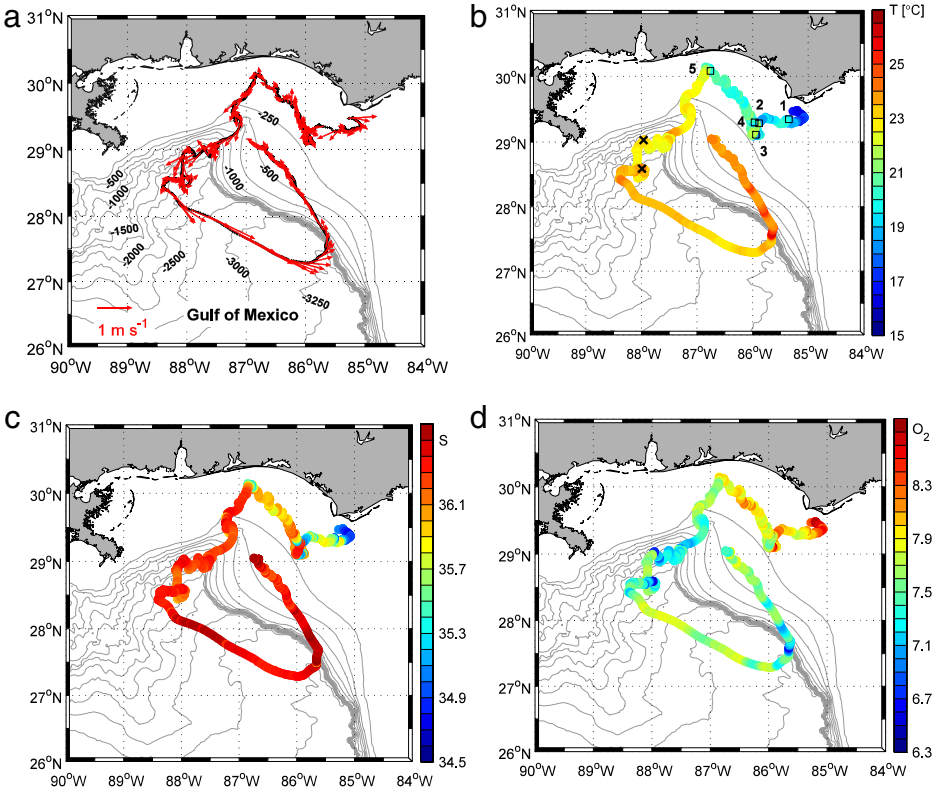

Fig. 2. (Upper) Ocean model domains and bathymetry; (Left) GoM-HYCOM regional model; (Right) NGoM-HYCOM nested model. (Lower) Sea Surface Height from GoM-HYCOM on 15 May 2013.

2.2. SailBuoy sensors and data reduction

The G-CTD sensor is a low-drag, fast-response unit composed of a 4-electrode conductivity cell and a stable thermistor. Schmitt and Petitt (2006) found that temperature and salinity measurements from the NBOSI G-CTD compare favorably with those from a co-located Sea-Bird Scientific G-CT (SBE 41). Because of its demonstrated accuracy, rugged design, low drag, and resistance to biofouling, the NBOSI G-CTD sensor is suitable for the SailBuoy. The serial port outputs temperature and conductivity data at a 5-Hz sample rate. The fin-cell was mounted on the hull of the SailBuoy about 15 cm below the water line (Fig. 1(c)). DC power at 12 VDC was supplied to the G-CTD board. A DC/DC converter then generated the ±5 VDC required by the board electronics. The board draws about 30 mA independent of the sample rate. The thermistor temperature sensor is calibrated by the manufacturer in a high-stability, temperature-controlled bath. Salinity is calculated from conductivity following Fofonoff and Millard (1983). The G-CTD sensor was delivered calibrated from the manufacturer. No post calibration was done at the end of the mission.

For oxygen measurements, the AS4835 optode, manufactured by Aanderaa Data Instruments, Xylem Inc., was fitted to the SailBuoy. This optode samples the dissolved O_2 concentration and air saturation at a resolution of 1 μm and 0.4%, respectively. The average current drain is $0.16 + 48$ mA/t where t is the sampling interval in seconds. The optode was mounted to the hull, on the opposite side of the G-CTD. The optode is capable of measurements for long-duration subsurface applications (Körtzinger et al., 2005), making it suitable for use on the SailBuoy. The operational principle of the optode is based on the ability of selected substances to act as dynamic fluorescence quenchers. Quenching refers to any process that decreases the fluorescence intensity of a given substance (Peng et al.,

2009). Dissolved oxygen in the water quenches both decay time and intensity of the luminescence emitted by a gas permeable foil that is exposed to the surrounding water. The sensor is coated by a black optical isolation for protection from incoming sunlight and fluorescent particles in the water.

The data were transmitted from the SailBuoy via the Iridium constellation at typically one hour intervals. Conductivity and temperature were sampled at 5 Hz for 8 s at the start of each sampling period. The batch of 40 data points for both temperature and conductivity were internally averaged after ignoring any outliers exceeding ± 1 standard deviation to remove the effects of possible spikes and erratic readings at the surface layer. The resulting mean values were relayed along with GPS fix, time stamp, and engineering data.

Near-surface conductivity measurements can be subjected to biofouling and spiking. Spikes are detected as follows. Seawater conductivity is strongly dependent on temperature (T), and when salinity variability does not dominate, temperature can be inferred from conductivity (C) using linear regression. Because the T sensor is relatively less susceptible to spiking and fouling, we detect and exclude erroneous conductivity data points by comparing the temperature recorded by the T sensor and that inferred from the C sensor. An erroneous data point is detected as an outlier when the difference from conductivity-inferred T is greater than twice the root-mean-square value. In total, 8 outliers (out of 1566 transmitted data points) were detected and replaced by linear interpolation. Finally, time series of location and *in situ* values were averaged to hourly intervals. Comparison of the SSS record with collocated Aquarius satellite SSS data indicates no evident biofouling or drift of the sensor. Absolutely no evidence of biofouling was observed when the SailBuoy was recovered.

2.3. Remote sensing data

The Moderate Resolution Imaging Spectroradiometers (MODIS) carried by NASA's Terra and Aqua satellites acquire data in 36 spectral channels from 0.415 to 14.235 μm, with a spatial resolution between 250 m and 1 km (Savtchenko et al., 2004). For our SST comparisons, the Aqua MODIS Level 3 global SST products were used to avoid any part of trajectories that are missing in Level 2 regional images. These are updated on the Ocean Color website on a daily basis (http://oceancolor.gsfc.nasa.gov).

Out of the 36 channels, only bands 31 and 32 in thermal-infrared (11.0–12.0 μm) are dedicated to the determination of SST (Savtchenko et al., 2004). The thermal-infrared bands have large bandwidths (used for MODIS product "SST"), which are close to the maximum level of the Earth's emission despite the fact that they are hindered by atmospheric water vapor absorption (Brown et al., 1999). A total of 62 Hierarchical Data Format (HDF) images were processed using two software packages: SeaDAS 7.0.2 from NASA Ocean Color, and VISAT from ESA (European Space Agency). MODIS images were analyzed to retrieve the SST values matching the SailBuoy's trajectory. All daily global products were downloaded sequentially. Using daily averaged positions and *in situ* values, we retrieved SST values from MODIS observations.

Salinity measurements from the Aquarius satellite (version 3.0) were obtained from the NASA Physical Oceanography Distributed Active Archive Center. Both Level 2 (along-track) and Level 3 (gridded to daily, 1° horizontal resolution) were used. Aquarius repeats its orbit every 7 days, and ground-tracks are spaced about 1° apart in the study region, so the data have gaps in both space and time. Data points within 50 km and 3 days of each SailBuoy measurement were extracted from the Level 2 dataset and averaged in order to compare with SailBuoy salinities.

2.4. NOAA buoys

In situ observations from three moored buoys that are owned and maintained by the National Data Buoy Center were used to validate the SailBuoy temperature data and assess local wind conditions. Hourly temperature and wind data buoys #42012 (30.065N, 87.555W), #42039 (28.794N, 86.006W), and #42040 (29.212N, 88.207W) were extracted for the study period (http://www.ndbc.noaa.gov). At each buoy, the temperature sensor was 0.6 m below the sea surface and the anemometer was at 5 m height.

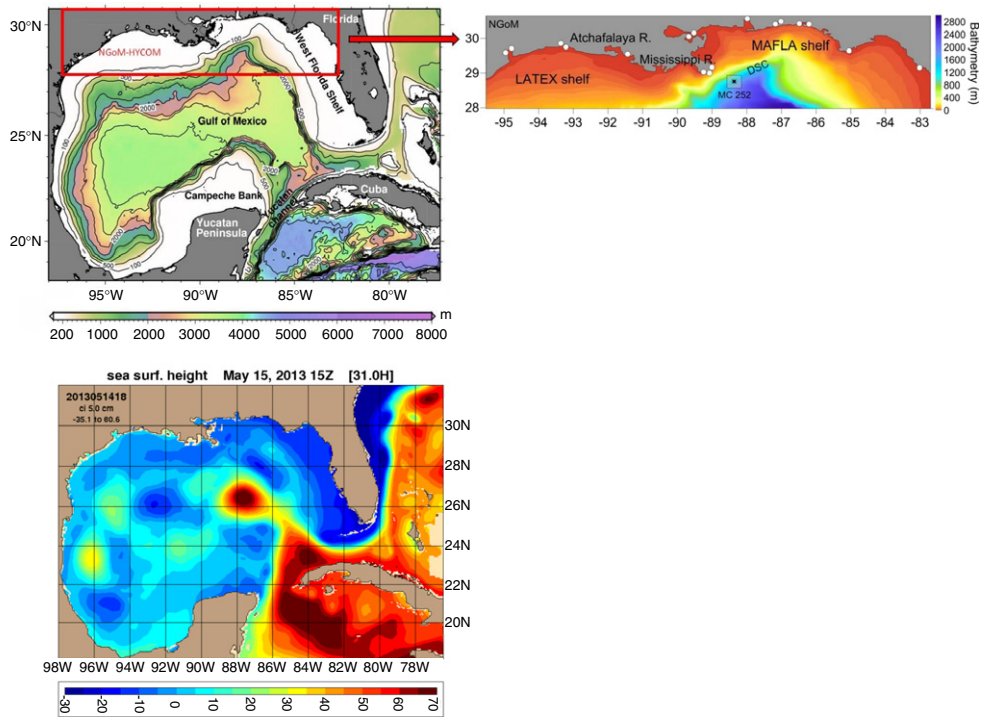

Fig. 3. Maps with the SailBuoy track showing (a) velocity vectors (every 7th data point), (b) temperature [° C], (c) salinity [Practical Salinity Units—PSU], and (d) oxygen concentration [mg/l]. The points 1 to 5 marked in (b) correspond to the location of the T/S anomalies. The two crosses mark the period between 24 April 18:00 and 28 April 18:00 UTC with the anomalous O_2 signal.

2.5. Ocean modeling system

Measurements from the SailBuoy have been combined with hydrodynamic model results to gain a better understanding of the oceanographic conditions during the field experiment and to demonstrate the usefulness of SailBuoy measurements to evaluate model results. SSS fields were chosen for the comparison, focusing on the major forcing mechanism that influences SSS variability in the study area, namely the evolution of the MR plume. A suitable modeling framework was chosen, based on the Hybrid Coordinate Ocean Model (HYCOM, see details at hycom.org), which has a special design for the vertical coordinate system that is optimized for topographically and dynamically complex domains such as the GoM (Schiller and Kourafalou, 2010). An existing modeling system based on HYCOM was chosen as it satisfies two relevant criteria: (a) data assimilative simulations of basin-wide dynamics (regional model); (b) coastal details and accurate parameterization of river plume dynamics (nested coastal model). Both models have been running for several years and have been shown to perform well against observations. The two system components are: (a) the regional Gulf of Mexico (GoM-HYCOM) and b) the nested Northern Gulf of Mexico (NGoM-HYCOM); see Fig. 3 for the model domains and topography and http://coastalmodeling.rsmas.miami.edu for more details. GoM-HYCOM has a horizontal grid resolution of ∼3.5 km and is data assimilative (using the US Navy Coupled Data Assimilation/NCODA system (Cummings, 2005)). It has been used in numerous applications and has shown accuracy in the evolution of the mesoscale dynamics, which can impact both deep and coastal GoM areas (Halliwell et al., 2009; Kourafalou et al., 2009; Le Hénaff et al., 2012a; Mariano et al., 2011; Cochrane, 1972; Leben, 2005).

The NGoM-HYCOM is free running, and has twice the horizontal resolution (∼1.8 km) and finer scale atmospheric forcing of GoM-HYCOM. An important difference between the two models, relevant

to the comparison with the SailBuoy data, is the treatment of river inputs. GoM-HYCOM uses monthly climatology for river discharges and also employs relaxation of salinity to climatology. NGoM-HYCOM is the only model in the study area that uses an advanced parameterization of river plume dynamics (Schiller and Kourafalou, 2010), which imposes both salinity and momentum fluxes at the rivers, high frequency (daily) discharge values, and no relaxation to climatological salinity values. As such, it is optimized to provide realistic fields for salinity fronts created by the discharge of the NGoM Rivers, and especially the MR, as established through data based evaluation (Oey et al., 2005; Schmitz, 2005; Le Hénaff et al., 2012b).

An example of mesoscale dynamics that are relevant to the study results (Section 4.3) is given in Fig. 3, through a Sea Surface Height (SSH) map from GoM-HYCOM at the end of the experiment (15 May 2013). As is well known (Androulidakis and Kourafalou, 2013; Halliwell et al., 2009; Kourafalou et al., 2009; Le Hénaff et al., 2012a; Mariano et al., 2011), the GoM mesoscale dynamics are governed by the evolution of the Loop Current (LC, a component of the Gulf Stream system) and its associated eddy field. When the LC reaches its most extended position in the GoM, it sheds an anticyclonic ring (LC Eddy, or LCE), which moves westward while the LC retracts to a southward position. This process was taking place during 15 May 2013 (Fig. 3). Cyclonic frontal eddies (called LCFEs) travel around the LC main front, and their evolution contributes to the LCE shedding process. Such an LCFE is also seen in the SSH field of Fig. 2, northeast of the LC front. These basin-wide processes impact the shelf dynamics, where circulation is also buoyancy-driven (due to river input) and wind-driven. As will be discussed in the next section, the SailBuoy track was first influenced by the wind-driven currents (prior to 1 May), until it encountered deeper waters and was influenced by the LCFE cyclone.

3. Results

3.1. SailBuoy performance and measurements

Hourly position vectors were constructed as eastward and northward displacements of the SailBuoy, from which the velocity vector over ground is calculated. Fig. 2(a) shows the track of the SailBuoy together with the inferred velocity vectors. Prior to 1 May 2013 (1139 data points) the average and standard deviation of the speed over ground (from GPS positions) is 37 $\pm$24 cm s^{-1} with a maximum of 143 cm s^{-1}. As will be further discussed in Section 4.3, this is a wind-driven period, followed by a period of influence by the cyclonic eddy (Section 2.4). Prior to 1 May, the average wind speed at NOAA Buoy #42039 was 6.5 m/s, while in the latter period it was 6 m/s. In the first period the wind was predominately easterly and the SailBuoy navigated with a head wind, while in the second a northerly component dominated and the SailBuoy navigated with a side wind. Statistics are very similar for the neighboring NOAA Buoys #42012 and #42040 and are within 0.5 m/s in mean wind speed, indicating a horizontally homogeneous wind field. The head winds imply that the SailBuoy was required to tack frequently, and thus explains the lower speed in the first period. During the eddy-influenced second period (427 data points), the average and standard deviation of the ground speed are 55 $\pm$ 41 cm s^{-1} with a maximum of 181 cm s^{-1}. During this period, the SailBuoy traveled with a speed over 1 m s^{-1} in 13% of the time and with a speed over 0.5 m s^{-1} in 43% of the time. The presence of the counter-rotating anticyclonic and cyclonic eddy pair seen in the SSH field of Fig. 3 (the LCE and LCFE, see Section 2.4) created increased velocities in the front between them. Accordingly, the speed of the SailBuoy increased in this region, as it was advected by the surface circulation.

Near-surface temperature, salinity and O_2 measured by the SailBuoy are shown along the track of the vessel in Fig. 2. The measured values range between 16 and 26 °C, 34.6 and 36.6, and 6.7 and 8.5 mg/l for SST, SSS and O_2, respectively.

The temperature–salinity diagram, color coded for oxygen concentration (Fig. 4), shows that a low oxygen concentration was associated with warm and saline surface water whereas there was a gradual transition toward high oxygen concentration in cold and less saline waters.

Time series of temperature, conductivity, and salinity show no apparent drift or biofouling over the two month long deployment period (Fig. 5). The temperature varies between 16.0 and 25.9 °C; the typical rms variations after removing a linear trend is 0.9 °C. The trend is representative of the seasonal surface warming throughout the deployment period. Small-scale variability in the GoM is

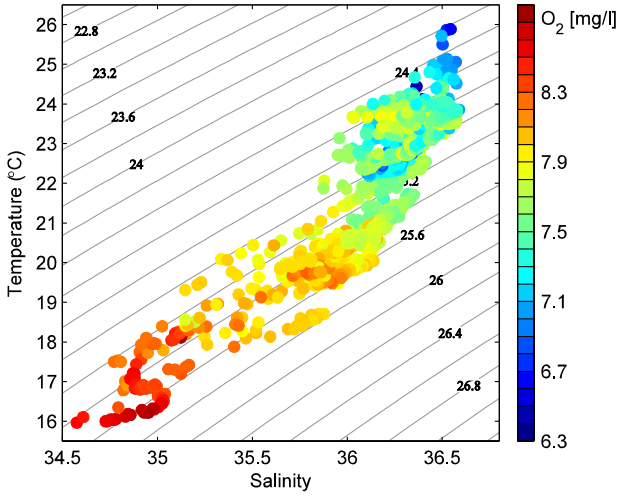

Fig. 4. Temperature–salinity diagram color-coded for dissolved oxygen concentration. Isolines are the potential density anomaly contours referenced to the surface pressure.

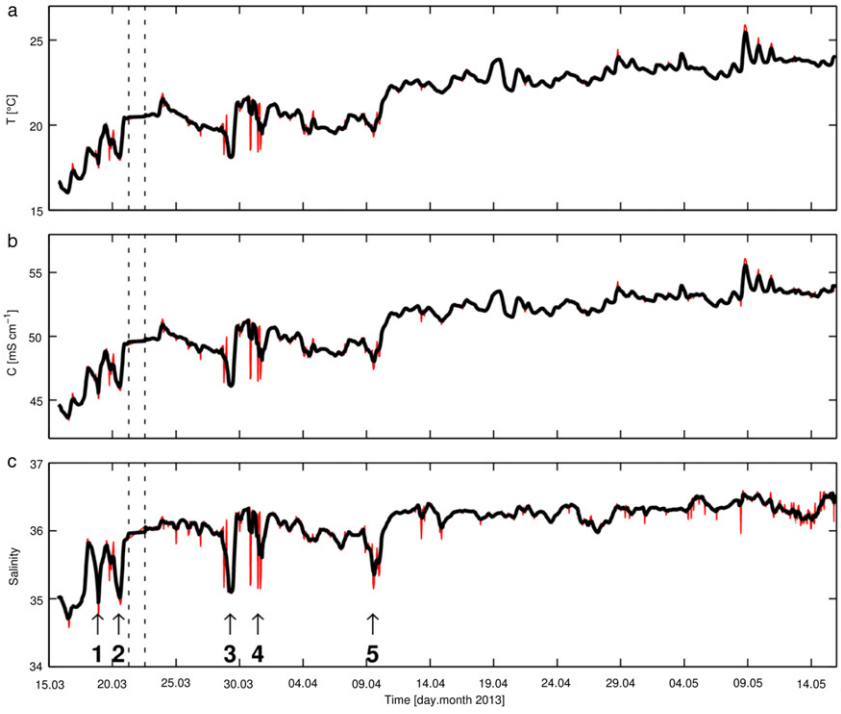

Fig. 5. Time series of (a) temperature, (b) conductivity, and (c) salinity. Red traces are the full resolution data, black traces are 7 point moving-averaged time series. Vertical dashed lines mark the period when the data acquisition was interrupted; the linearly interpolated data in this period must be interpreted with caution. The times of temperature and salinity anomalies mentioned in the text are marked by arrows 1 to 5. (For interpretation of the references to color in this figure legend, the reader is referred to the web version of this article.)

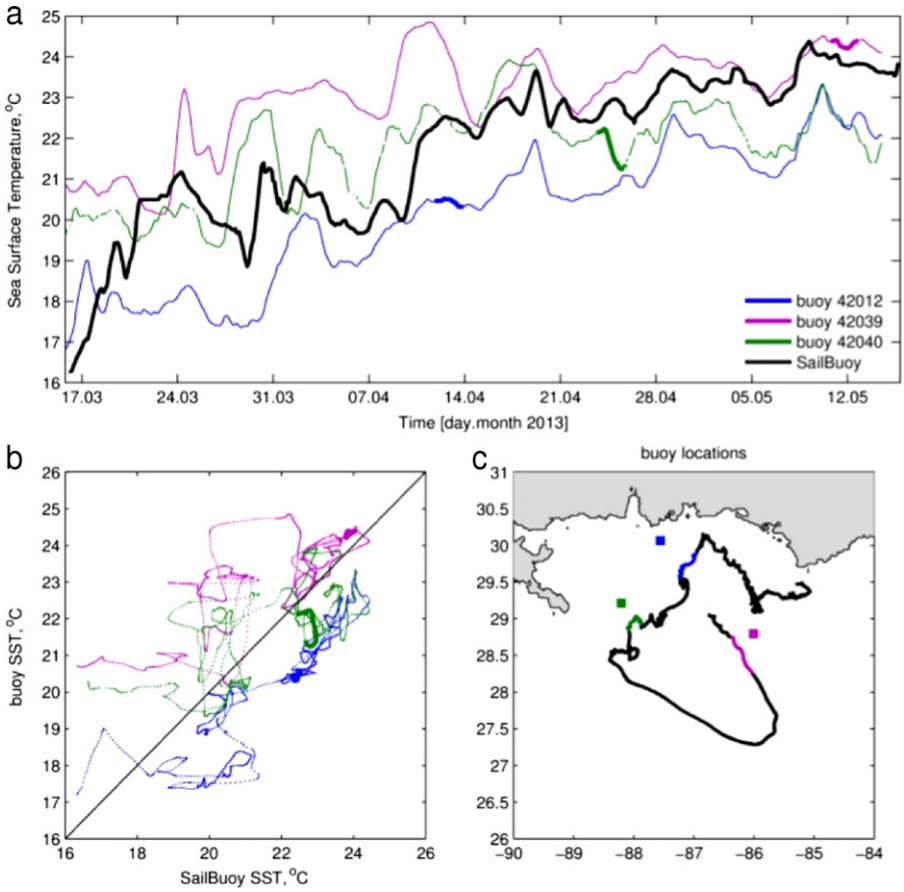

Fig. 6. Comparison of SST from the SailBuoy and from NOAA buoys in the northeastern GoM. (a) Temperature time series during the study period, with the SailBuoy shown in black; (b) scatterplot of buoy SSTs plotted against SailBuoy SST. For (a) and (b), the hourly time series were smoothed with a 24-hour running mean to remove diurnal variations; for each NOAA buoy, data for which the SailBuoy was within 150 km of a given buoy are plotted as thick lines. (c) Study region showing the SailBuoy track (black) and the NOAA buoy locations (colored squares). (For interpretation of the references to color in this figure legend, the reader is referred to the web version of this article.)

strong, which makes it difficult to compare observations made using a moving platform against buoy data at a fixed location. However, comparison of SailBuoy temperatures (smoothed using a 24-hour running mean) with near-surface temperature from nearby NOAA surface buoys illustrates that many of the prominent features captured by the SailBuoy are seen elsewhere in the eastern GoM (Fig. 6). For example, the temperature peak around 18 April is observed at NOAA buoy #42012, which the SailBuoy was near at the time; a similar temperature anomaly from 28 April to 5 May is seen in data both from the SailBuoy and from buoy #42040. At the time of nearest approach to the buoys (52 km for buoy #42012, 33 km and 31 km for the two times that the SailBuoy approached buoy #42039, and 31 km for buoy #42040), the absolute values of the buoy data do not always agree well with the SailBuoy, likely because mesoscale and submesoscale variability in this region are strong as a result of the river plume. However, this comparison nonetheless demonstrates that the SailBuoy captures both the temporal warming trend as well as many prominent temperature features.

The calculated salinity varies by 2 practical salinity units, between 34.6 and 36.6. This also coincides with the transition from coastal and river-influenced waters to offshore more saline waters and Loop current dominated waters known to have an even higher salt concentration. The high-frequency

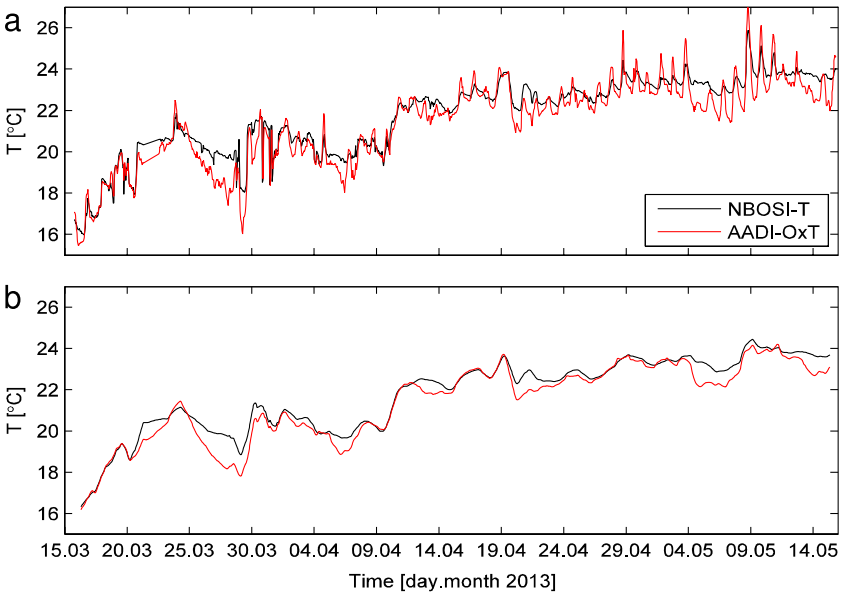

Fig. 7. Time series of temperature measured by the NBOSI-T sensor (black) and the temperature sensor on the oxygen optode (OxT, red) using (a) all data points and (b) daily running mean after gridding to 1-hour intervals.

variability in surface temperature and salinity is dominated by coherent decrease in T and S seen at several locations. This is presumably due to spatial variability as the SailBuoy sampled across less saline/cold shelf and saline/warm offshore surface water. The strongest T/S anomalies (marked as 1 to 4 in Fig. 5) are measured on 18 March, 20 March, 29 March, and 31 March, with typical decreases of approximately 0.6–1 in salinity and 0.7–2 °C in temperature lasting for approximately 1–2 days. Finally, there is a dip on 9 April noon (event 5) followed by a transition to warmer and saline waters as the SailBuoy crossed a front where salinity and temperature increased by approximately 0.7 and 2 °C, respectively. In the remainder of the dataset, typical fluctuations are about 0.2 in S and less than 1 °C in T.

Ancillary temperature measurements made by the optode confirm that the increase in temperature throughout the experiment is not due to sensor drift. In Fig. 7 we compare the temperature recorded by the NBOSI sensor with that recorded by the optode (OxT). The OxT sensor is in the optode and therefore has a slow time response; it heats up and cools with the hull of the SailBuoy, as can be seen in the diurnal fluctuations in the time series. A comparison of the two temperature time series (after applying a daily moving average) shows good agreement with no apparent drift, suggesting high quality temperature measurements over the 2-month duration of the experiment. The temperature anomalies associated with events 1 to 5 identified in Fig. 5 can also be seen in the OxT record. The density-compensating nature of the anomalies, the agreement between NBOSI-T and OxT records, and the 1–2 day duration of the events together suggest that these events are not spikes, but rather coherent signals associated with features such as mesoscale fronts or sub-mesoscale filaments.

Time series of dissolved oxygen concentration and O_2 air saturation are shown in Fig. 8. There is a substantial diurnal variability. The diurnal variability is expected as a result of photosynthesis and aerobic respiration. During the day, oxygen production by photosynthesis causes an increase in dissolved oxygen, whereas algal, microbial, and plant respiration at night consumes oxygen. Between 24 April 18:00 and 28 April 18:00 UTC an anomalous O_2 signal with elevated concentrations can be seen. The position of the SailBuoy during this period as well as during the TS anomaly events is marked on the temperature map (Fig. 2(b)). This anomalous signal cannot be explained by biofouling which would lead to a gradual decrease in the measurements, rather than the abrupt increase that

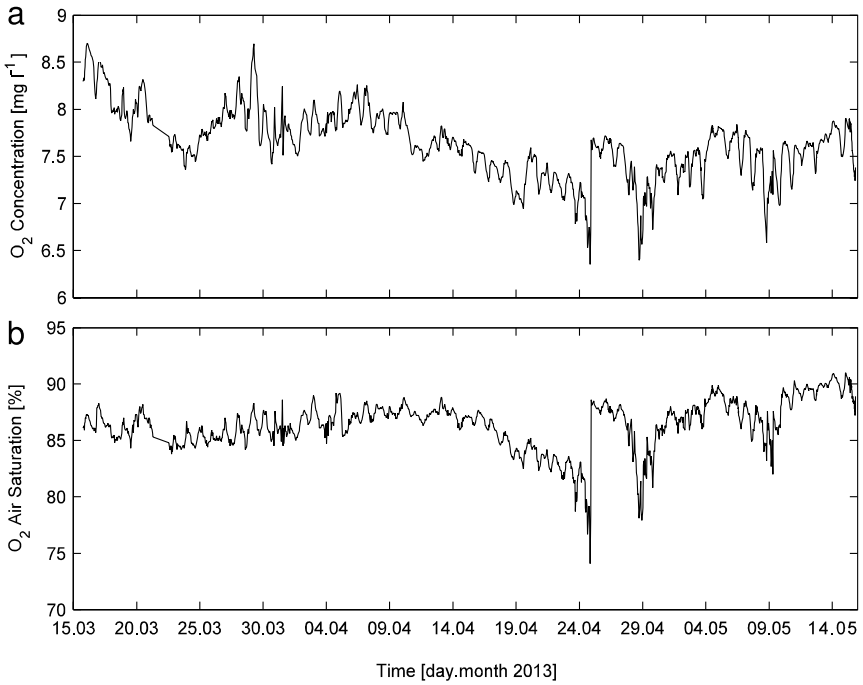

Fig. 8. Time series of (a) dissolved oxygen concentration and (b) oxygen air saturation.

was observed. Given the large spatial variability at the site, this signal is most likely natural, related to a patch with higher biologic production. It is also possible that at an earlier time (mid April) something stuck on the sensor, yielding low O_2 concentrations, which was eventually washed out at the time of the event, increasing the O_2 back to higher concentrations. We dismiss this alternative, however, as it does not explain the second dip in the measurements that occurred at the end of April. Tengberg et al. (2006) conducted a comprehensive evaluation of the Aanderaa Data Instruments optodes for long term *in situ* measurements in different environments such as estuarine, river, waste water, and ocean. They report satisfactory long-term stability and performance. In heavy fouling environments, they recommend wrapping a beryllium–copper alloy net around the sensor, which slows down fouling of the optode from approximately 7 to 10 days to 40 to 60 days.

3.2. Comparison to remote sensing data

Daily averaged SailBuoy SST values compare well with the daily averaged MODIS Terra (day/night) SST values (Fig. 9). Satellite SST agrees with the observed trend, which represents the surface warming throughout the deployment period. Time-averaged values are 22.6 °C and 22.5 °C for the SailBuoy and satellite, respectively, demonstrating an agreement within the uncertainties on each variable. Satellite-inferred daily SST typically captures the daily SailBuoy SST observations to within less than 1 °C. Occasionally, such as in early and late April, MODIS underestimates the SST by 2 to 3 °C, likely because satellite SSTs are averaged over a large spatio-temporal region compared to the point measurements made by the SailBuoy, so local SST anomalies due to small-scale features may not be sampled by the satellite.

Fig. 10(a) shows the ground-track of the Aquarius satellite passes in the study region, colored by the Aquarius salinities observed from 15 March to 15 May 2013. Each colored point represents a single Aquarius measurement; note, however, that the "footprint" of the satellite is around 100 km (Lagerloef et al., 2008), so adjacent observations overlap considerably in the area they represent. The Aquarius radiometers are adversely affected by measurements over land, so only data more than 100 km away

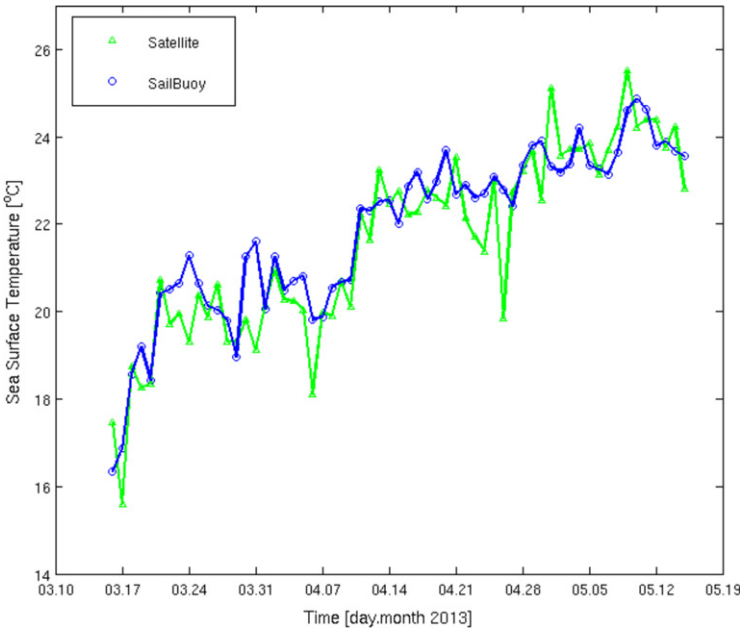

Fig. 9. Daily-averaged time series of SST measured by the SailBuoy and inferred from MODIS Terra (day/night).

from the coast are considered. Fig. 10(b) shows salinities from the SailBuoy as well as from the Level 2 (along-track) and Level 3 (gridded) Aquarius products, where the Level 2 data were subsampled to the time and location of the SailBuoy whereas the Level 3 data are of coarser resolution and are centered on 28N, 87W. The Aquarius data are too coarse in space and time to resolve small-scale features observed with the SailBuoy. However, away from the coast, the level 3 Aquarius salinities agree well with the SailBuoy observations, though the Level 2 data have somewhat higher values (Fig. 10(b)).

3.3. Comparison to hydrodynamic model outputs

Finally, measured SSS values from the spring 2013 deployment (Section 2.1) were compared with the HYCOM modeling system described in Section 2.4. This is an interesting comparison for two reasons. Firstly, the GoM regional model covers the deep SailBuoy pathway (2nd phase, discussed in Section 4.1), while the NGoM coastal model covers the shelf and shelf-break, primarily wind-driven 1st phase (discussed here). Secondly, the two models have a substantially different parameterization of river forcing and thus produce different SSS fields. The GoM model is primarily capable of reproducing monthly cycles, while the NGoM model can also accurately represent shorter term SSS variability, which is important for this study. Therefore, the SSS comparison with both models indicates whether the SailBuoy better captures "average" or small-scale salinity features.

Time series of model results were extracted along the SailBuoy track, with a focus on the period when the experiment was dedicated to the mapping of the Mississippi River plume. The related track (April 21–30) is shown in Fig. 11, with SSS values measured by the SailBuoy superimposed. The high salinity values captured by the SailBuoy indicate that the Mississippi waters had not influenced the study area during that period. For comparison, snapshots of model fields on April 15 (∼middle of the SailBuoy track period) are shown for the two models. The comparison indicates excellent agreement between the SailBuoy measurements and the nested NGoM-HYCOM model (Fig. 11(b)), which has the most accurate representation of the Mississippi River plume influence (see Section 2.4). The model confirms that high SSS values measured by the SailBuoy correspond to the absence of Mississippi waters in the area, as the plume was deflected westward rather than offshore during

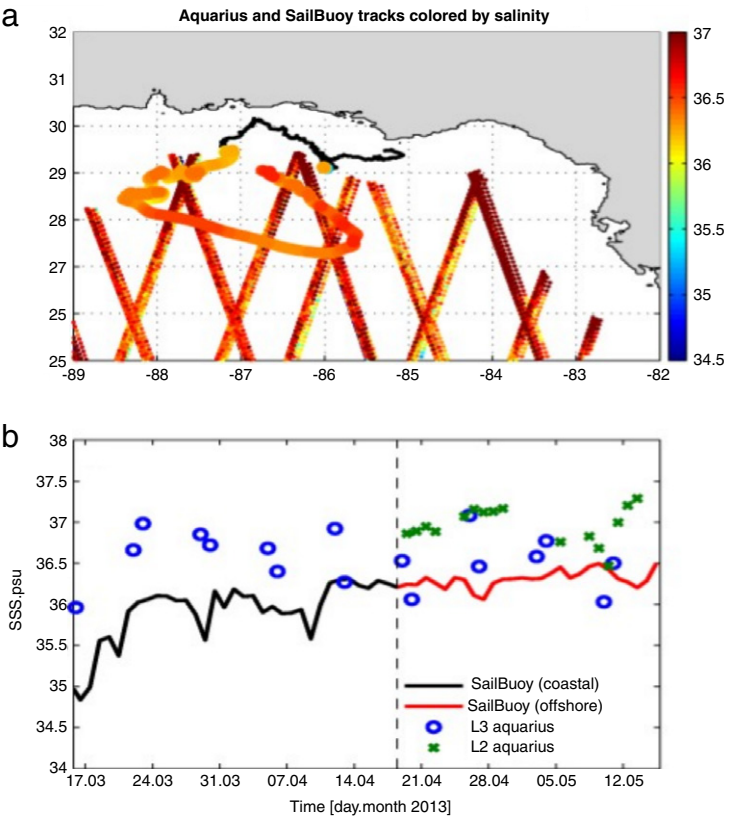

Fig. 10. (Upper) Sail Buoy track for April 21–30 (2013), approaching the DeSoto canyon and the region of Mississippi plume influence; (Middle) Sea Surface Salinity (SSS) computed by the high resolution Northern GoM nested model (NGoM-HYCOM); (Bottom) Sea Surface Salinity (SSS) computed by the regional model (GoM-HYCOM). Sailbuoy track salinity data are marked by red circles on the model SSS fields. (For interpretation of the references to color in this figure legend, the reader is referred to the web version of this article.)

the experiment period. The SailBuoy was thus in waters away from the Mississippi River influence. Conversely, the regional GoM-HYCOM model having a climatological representation of the river input produces an erroneous distribution of the Mississippi River waters, as seen by poor agreement with salinity measured by the SailBuoy (Fig. 11(c)).

4. Discussion

The fundamental difference between the SailBuoy and drifters or buoys is the operating procedure. The vessel navigates toward pre-defined waypoints that are sent to it via the Iridium network. During this experiment, the SailBuoy successfully reached each waypoint, demonstrating the efficacy of this approach. Another possible mode of operation is for the vessel to hold position at a single location, allowing quasi-stationary measurements to be made without any anchoring. This makes the SailBuoy advantageous over freely drifting systems like drifters and buoys.

Power supply or consumption is a concern for many autonomous vehicles; power is often provided by diesel generators or charged sets of batteries. In comparison, the SailBuoy is a relatively light autonomous system, carrying two sets of batteries: one for the sensors and one back-up, which ensure at least a six month traveling capacity without needing to be serviced. The power supply could be

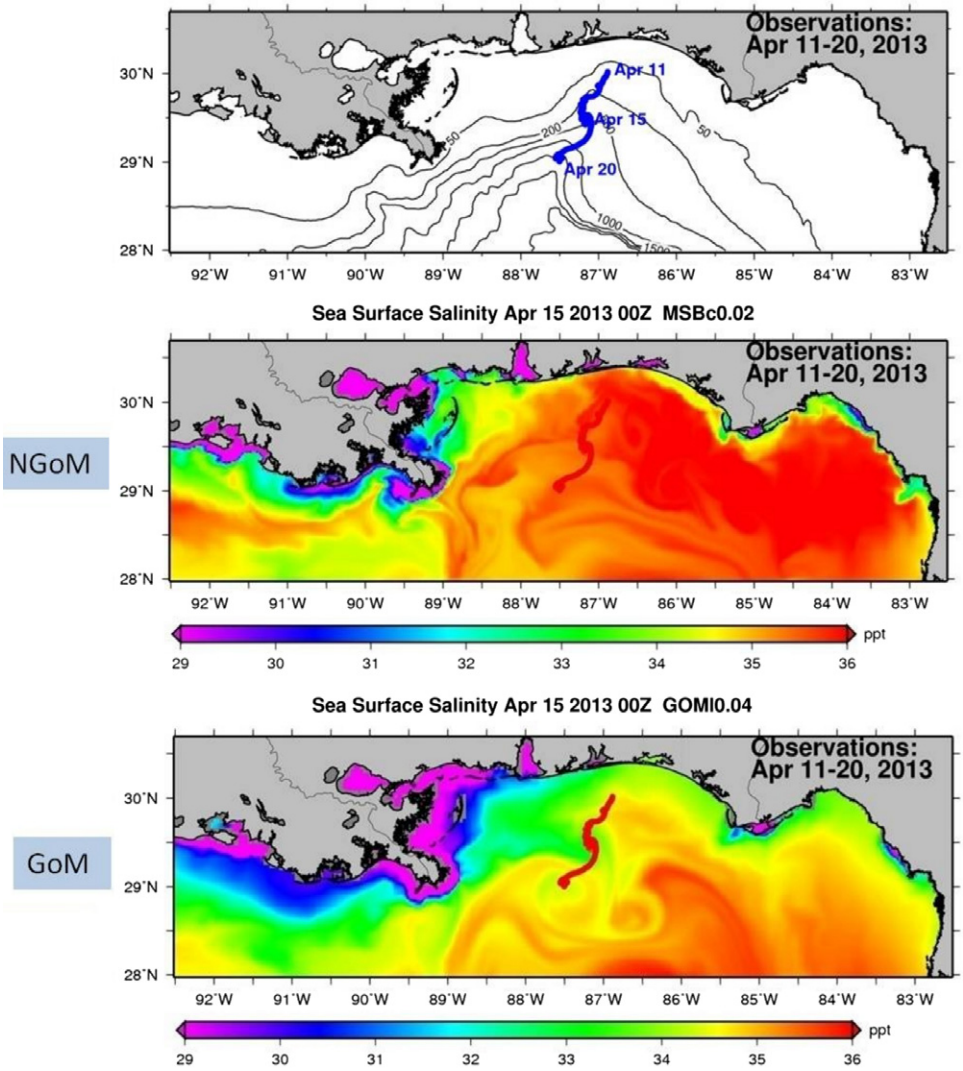

Fig. 11. (Upper) Sail Buoy track for April 21–30 (2013), approaching the DeSoto canyon and the region of Mississippi plume influence; (Middle) Sea Surface Salinity (SSS) computed by the high resolution Northern GoM nested model (NGoM-HYCOM); (Bottom) Sea Surface Salinity (SSS) computed by the regional model (GoM-HYCOM). Sailbuoy track salinity data are marked by red circles on the model SSS fields. (For interpretation of the references to color in this figure legend, the reader is referred to the web version of this article.)

further extended by installing a solar panel and a larger battery. The main challenge during very long missions would be biofouling on the sensors.

Near-surface ocean measurements in regions of fresh water influence, coastal waters and river plumes are challenging and costly when using either conventional research vessels or satellite remote sensing: the river plume undergoes rapid changes that are hard to follow under the usual ship time requirements, while satellite measurements of SSS in coastal waters are still very limited. The SailBuoy serves as a reliable alternative for deployment in such applications.

The model comparison exhibits the validity and usefulness of SailBuoy measurements in both shelf and deep oceanic regions and the instrument's utility in evaluating fields produced by ocean

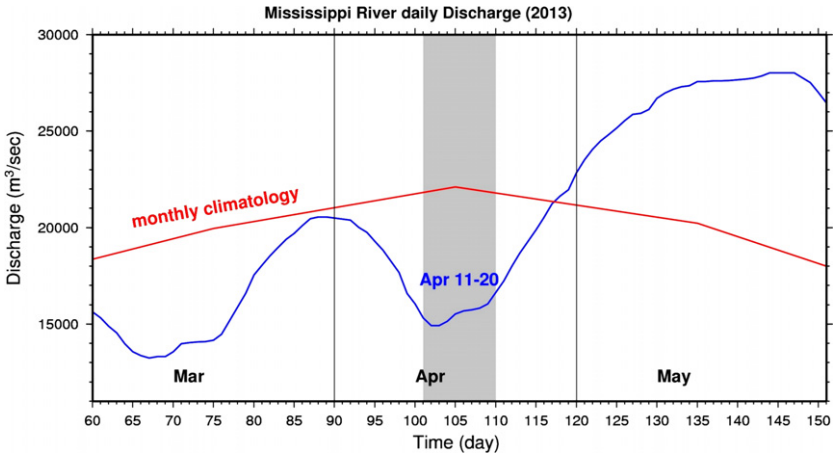

Fig. 12. Daily average discharge from the Mississippi in the spring of 2013 (blue line) compared to monthly climatology (red line). The period of 11–20 April (gray highlight) corresponds to the model SSS panels shown in Fig. 10. (For interpretation of the references to color in this figure legend, the reader is referred to the web version of this article.)

models having different attributes. To better understand these results, the variability in MR discharge and the wind field are given in Figs. 12 and 13, respectively. The period 11–20 April exhibited a substantial difference between monthly climatology (represented by the regional GoM model) and daily discharge values (represented by the coastal NGoM model, which also has a more accurate representation of the evolution of the MR plume). This was reflected in the model computed SSS fields, which presented an overestimation of low salinity by the GoM model around the SailBuoy pathway, but realistically higher salinities by the NGoM model, which were accurately reflected in the SailBuoy measurements. The wind-driven currents that influenced the SailBuoy trajectory (superimposed on model SSS in Fig. 10 and also shown in Fig. 3) were influenced by the prevailing winds (Fig. 12). These were mainly from the south (southerlies) during the start of the low discharge period (11 April), shifting to light westerlies (15 April) and strong northerlies (20 April). These patterns are derived from the high resolution NGoM model forcing, based on 3-hourly atmospheric fields of the US Navy's Coupled Ocean–Atmosphere Prediction System (Hodur, 1997). COAMPS assimilates all ocean buoy data, including those mentioned in Section 4.1.

5. Summary and conclusions

The SailBuoy offers the capabilities of an unmanned autonomous oceanic vehicle which can be used as a new generation system for *in situ* near-surface data collection at sea. This is demonstrated by a recent experiment conducted in the Gulf of Mexico. The dataset retrieved from this mission is comprised of sea surface temperature, conductivity and dissolved oxygen concentration, as well as the position of the vessel. The vessel speed is inferred from its displacement between adjacent measurements and the known time stamps. Measurements of temperature, salinity and oxygen are found to be of high quality with no apparent drift or biofouling over the two-month deployment period. The instrument sampled across fronts between the shelf and offshore waters in the Gulf of Mexico in the early part of the record, and then looped clockwise toward the northeast part of the basin. The shelf is characterized by cold, low salinity, oxygen rich waters. Off the shelf we find surface waters with relatively higher temperature and salinity, but lower oxygen concentration. The data show variability of typically 0.2 in salinity and less than 1 °C in temperature.

A comparison with the results from a regional/coastal ocean circulation modeling system exhibits the usefulness of SailBuoy measurements and the instrument's utility in evaluating fields produced by ocean models of different attributes. In addition, the circulation deduced by data assimilative oceanographic and atmospheric models was correctly followed by the SailBuoy, which was influenced

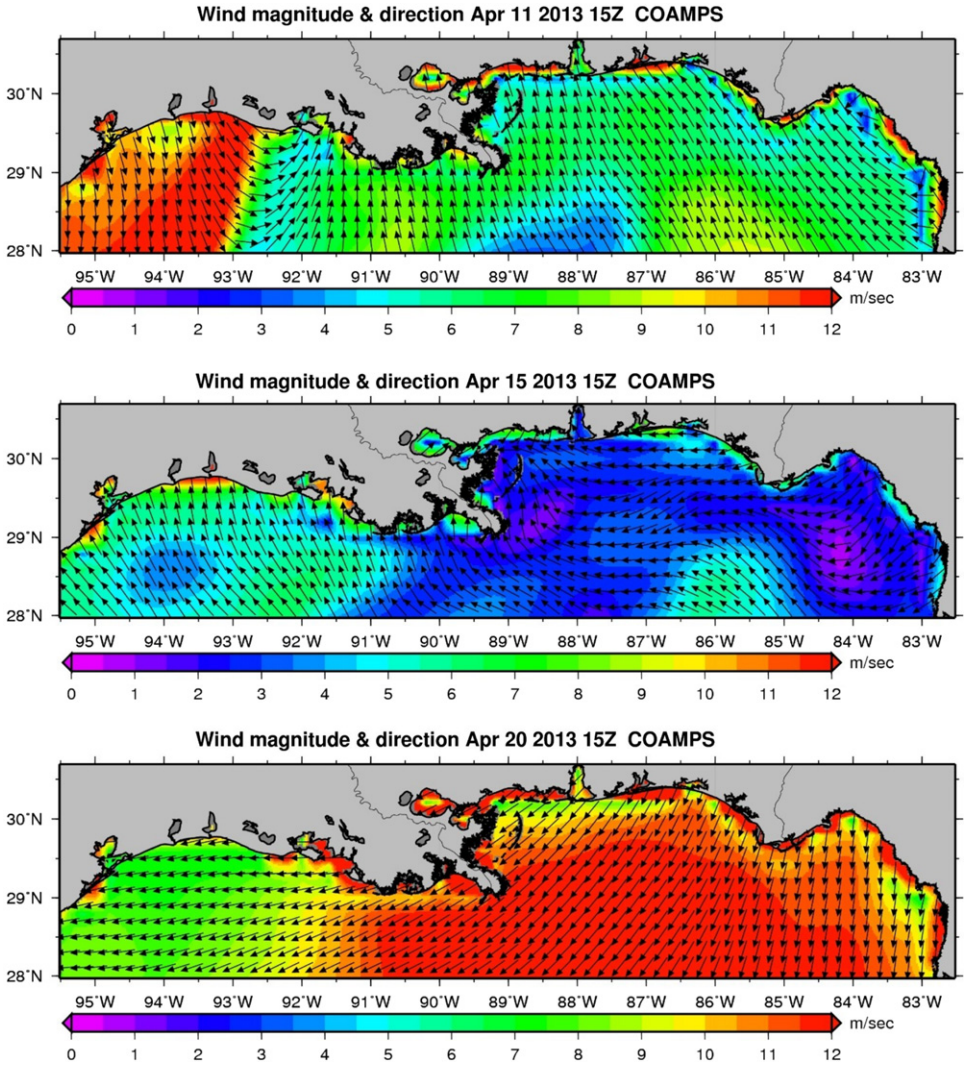

Fig. 13. Wind magnitude (in m/s, color scale) and direction (vectors) over the NGoM-HYCOM model domain; data from the US Navy COAMPS (Coupled Ocean–Atmosphere Mesoscale Prediction System). Snapshots are provided for 15Z on the 11th (upper), 15th (middle) and 20th (lower), of April 2013. (For interpretation of the references to color in this figure legend, the reader is referred to the web version of this article.)

by both shelf wind-driven and deep oceanic mesoscale features. A small unmanned marine vehicle such as the SailBuoy poses limited danger to commercial navigation traffic. Year-long missions are possible to remote and even dangerous regions with no human risk involved. A fleet of unmanned remotely-controlled vessels may be a cost- and time-efficient tool for ocean observations and monitoring at large scale.

Acknowledgments

This research was made possible by a grant from BP/The Gulf of Mexico Research Initiative to the Deep-C consortium. The field study has been conducted in collaboration between Florida State University, Christian Michelsen Research and the Norwegian Meteorological Institute, Bergen.

References

Androulidakis, Y.S., Kourafalou, V.H., 2013. On the processes that influence the transport and fate of Mississippi waters under flooding outflow conditions. Ocean Dyn. 63 (2–3), 143–164.

Brown, O.B., Minnett, P.J., Evans, R., Kearns, E., Kilpatrick, K., Kumar, A., Závody, A., 1999. MODIS Infrared Sea Surface Temperature Algorithm Algorithm Theoretical Basis Document Version 2.0.. University of Miami, 33149-1098.

Caccia, M., Bibuli, M., Bono, R., Bruzzone, G., 2008. Basic navigation, guidance and control of an unmanned surface vehicle. Auton. Robots 25 (4), 349–365.

Caccia, M., Bono, R., Bruzzone, G., Spirandelli, E., Veruggio, G., Stortini, A.M., Capodaglio, G., 2005. Sampling sea surfaces with SESAMO: an autonomous craft for the study of sea-air interactions. IEEE Robot. Autom. Mag. 12 (3), 95–105.

Cochrane, J.D., 1972. Separation of an anticyclone and subsequent developments in the Loop Current (1969). Contributions on the Physical Oceanography of the Gulf of Mexico 2, 91–106.

Cummings, J.A., 2005. Operational multivariate ocean data assimilation. Quart. J. Royal Met. Soc. 131, 3583–3604.

Fer, I., Peddie, D., 2012. Near-surface oceanographic measurements using the Sail Buoy: test deployment off Grand Canaria, Christian Michelsen Research AS, Bergen, Rep. No. CMR-13-A10266-RA-2. 15 pp.

Fofonoff, N.P., Millard, R.C., 1983. Algorithms for computation of fundamental properties of seawater.

Halliwell Jr, G.R., Barth, A., Weisberg, R.H., Hogan, P., Smedstad, O.M., Cummings, J., 2009. Impact of GODAE products on nested HYCOM simulations of the West Florida Shelf. Ocean Dyn. 59 (1), 139–155.

Hamilton, P., Berger, T.J., Singer, J.J., Waddell, E., Churchill, J.H., Leben, R.R., Sturges, W., 2000. DeSoto Canyon eddy intrusion study: Final report (pp. 20000-80). Volume II: Technical Report.

Hamilton, P., Lee, T.N., 2005. Eddies and jets over the slope of the northeast Gulf of Mexico. Circulation in the Gulf of Mexico: observations and models 123–142.

Hodur, R.M., 1997. The Naval Research Laboratory's coupled ocean/atmosphere mesoscale prediction system (COAMPS). Mon. Weather Rev. 125 (7), 1414–1430.

Huh, O.K., Wiseman, W.J., Rouse, L.J., 1981. Intrusion of Loop Current waters onto the west Florida continental shelf. J. Geophys. Res.: Oceans (1978–2012) 86 (C5), 4186–4192.

Joos, F., Plattner, G.K., Stocker, T.F., Körtzinger, A., Wallace, D.W., 2003. Trends in marine dissolved oxygen: implications for ocean circulation changes and the carbon budget. Eos, Trans. Amer. Geophys. Union 84 (21), 197–201.

Körtzinger, A., Schimanski, J., Send, U., 2005. High quality oxygen measurements from profiling floats: a promising new technique. J. Atmos. Ocean. Technol. 22 (3), 302–308.

Kourafalou, V.H., Peng, G., Kang, H., Hogan, P.J., Smedstad, O.M., Weisberg, R.H., 2009. Evaluation of global ocean data assimilation experiment products on South Florida nested simulations with the Hybrid Coordinate Ocean Model. Ocean Dyn. 59 (1), 47–66.

Lagerloef, G., Colomb, F.R., Le Vine, D., Wentz, F., Yueh, S., Ruf, C., Chao, Y., deCharon, A., Feldman, G., Swift, C., 2008. The Aquarius/SAC-D mission: Designed to meet the salinity remote-sensing challenge. Oceanography 21 (1), 68–81.

Leben, R.R., 2005. Altimeter-derived loop current metrics. Circulation in the Gulf of Mexico: Observations and Models 181–201.

Le Hénaff, M., Kourafalou, V.H., Morel, Y., Srinivasan, A., 2012b. Simulating the dynamics and intensification of cyclonic Loop Current Frontal Eddies in the Gulf of Mexico. J. Geophys. Res.: Oceans 117 (1978–2012), C2.

Le Hénaff, M., Kourafalou, V.H., Paris, C.B., Helgers, J., Aman, Z.M., Hogan, P.J., Srinivasan, A., 2012a. Surface evolution of the Deepwater Horizon oil spill patch: combined effects of circulation and wind-induced drift. Environ. Sci. Technol. 46 (13), 7267–7273.

Lenain, L., Melville, W.K., 2014. Autonomous surface vehicle measurements of the ocean's response to tropical cyclone Freda. J. Atmos. Ocean. Technol. (2014).

Manley, J.E., 1997. Development of the autonomous surface craft ACES. In: OCEANS'97 MTS/IEEE Conference Proceedings vol. 2. IEEE, pp. 827–832. October.

Mariano, A.J., Kourafalou, V.H., Srinivasan, A., Kang, H., Halliwell, G.R., Ryan, E.H., Roffer, M., 2011. On the modeling of the 2010 Gulf of Mexico oil spill. Dyn. Atmos. Oceans 52 (1), 322–340.

Oey, L.Y., Ezer, T., Lee, H.C., 2005. Loop Current, rings and related circulation in the Gulf of Mexico: a review of numerical models and future challenges. Circulation in the Gulf of Mexico: Observations and Models 31–56.

Pascoal, A., Oliveira, P., Silvestre, C., Sebastião, L., Rufino, M., Barroso, V., Dando, P., 2000. Robotic ocean vehicles for marine science applications: the european asimov project. In: Oceans 2000 MTS/IEEE Conference and Exhibition Vol. 1. IEEE, pp. 409–415.

Peng, X., Chen, H., Draney, D.R., Volcheck, W., Schutz-Geschwender, A., Olive, D.M., 2009. A nonfluorescent, broad-range quencher dye for Förster resonance energy transfer assays. Analyt. Biochem. 388 (2), 220–228.

Savtchenko, A., Ouzounov, D., Ahmad, S., Acker, J., Leptoukh, G., Koziana, J., Nickless, D., 2004. Terra and Aqua MODIS products available from NASA GES DAAC. Adv. Space Res. 34 (4), 710–714.

Schiller, R.V., Kourafalou, V.H., 2010. Modeling river plume dynamics with the HYbrid Coordinate Ocean Model. Ocean Modelling 33 (1), 101–117.

Schmitt, R.W., Petitt, R.A., 2006. A fast response, stable CTD for gliders and AUVs. In: OCEANS 2006. IEEE, pp. 1–5. September.

Schmitz, W.J., 2005. Cyclones and westward propagation in the shedding of anticyclonic rings from the Loop Current. Circulation in the Gulf of Mexico: Observations and Models 241–261.

Tengberg, A., Hovdenes, J., Andersson, H., Brocandel, O., Diaz, R., Hebert, D., Stangelmayer, A., 2006. Evaluation of a lifetime-based optode to measure oxygen in aquatic systems. Limnol. Oceanogr. Methods 4, 7–17.

Vukovich, F.M., 2007. Climatology of ocean features in the Gulf of Mexico using satellite remote sensing data. J. Phys. Oceanogr. 37 (3), 689–707.

Wang, D.P., Oey, L.Y., Ezer, T., Hamilton, P., 2003. Near-surface currents in DeSoto Canyon (1997–99): Comparison of current meters, satellite observation, and model simulation. J. Phys. Oceanogr. 33 (1), 313–326.